Physics Letters B 769 (2017) 339–344

Contents lists available at ScienceDirect

Physics Letters B

www.elsevier.com/locate/physletb

Isovector excitations in ^{100}Nb and their decays by neutron emission studied via the ^{100}Mo$(t, {}^3\mathrm{He} + n)$ reaction at 115 MeV/u

K. Miki [a,*], R.G.T. Zegers [a,b,c,*], Sam M. Austin [a,b], D. Bazin [a], B.A. Brown [a,b,c], A.C. Dombos [a,b,c], R.K. Grzywacz [d], M.N. Harakeh [e], E. Kwan [a], S.N. Liddick [a,f], S. Lipschutz [a,b,c], E. Litvinova [g,a,b], M. Madurga [d], M.T. Mustonen [h], W.J. Ong [a,b,c], S.V. Paulauskas [a], G. Perdikakis [i,a,b], J. Pereira [a,b], W.A. Peters [j,d,k], C. Robin [g,b], M. Scott [a,b,c], A. Spyrou [a,b,c], C. Sullivan [a,b,c], R. Titus [a,b,c]

[a] National Superconducting Cyclotron Laboratory, Michigan State University, East Lansing, MI 48824, USA
[b] Joint Institute for Nuclear Astrophysics, Center for the Evolution of the Elements, Michigan State University, East Lansing, MI 48824, USA
[c] Department of Physics and Astronomy, Michigan State University, East Lansing, MI 48824, USA
[d] Department of Physics and Astronomy, University of Tennessee, Knoxville, TN 37996, USA
[e] Kernfysisch Versneller Instituut, Center for Advanced Radiation Technology, University of Groningen, Groningen, 9747 AA, Netherlands
[f] Department of Chemistry, Michigan State University, East Lansing, MI 48824, USA
[g] Department of Physics, Western Michigan University, Kalamazoo, MI 49008, USA
[h] Center for Theoretical Physics, Sloane Physics Laboratory, Yale University, New Haven, CT 06502, USA
[i] Department of Physics, Central Michigan University, Mt. Pleasant, MI 48859, USA
[j] Oak Ridge Associated Universities, Oak Ridge, TN 37830, USA
[k] Physics Division, Oak Ridge National Laboratory, Oak Ridge, TN 37831, USA

ARTICLE INFO

Article history:
Received 27 November 2016
Received in revised form 15 March 2017
Accepted 4 April 2017
Available online 7 April 2017
Editor: D.F. Geesaman

Keywords:
Spin–isospin excitations
Neutron decay
Charge-exchange reaction
Missing mass spectroscopy

ABSTRACT

Spin–isospin excitations in ^{100}Nb were studied via the ^{100}Mo$(t, {}^3\mathrm{He})$ charge-exchange reaction at 115 MeV/u with the goal to constrain theoretical models used to describe the isovector spin response of nuclei. The experiment was performed with a secondary beam of tritons, and ^{3}He particles were analyzed in the S800 magnetic spectrometer. Decay by neutron emission from excited states in ^{100}Nb was observed by using plastic and liquid scintillator arrays. Differential cross sections were analyzed and monopole excitations were revealed by using a multipole decomposition analysis. The Gamow–Teller transition strength observed at low excitation energies, which is important for estimating the electron-capture rate in astrophysical scenarios, was strongly fragmented and reduced compared to single-particle and spherical mean-field models. The consideration of deformation in the theoretical estimates was found to be important to better describe the fragmentation and strengths. A strong excitation of the isovector spin giant monopole resonance was observed, and well reproduced by the mean-field models. Its presence makes the extraction of Gamow–Teller strengths at high excitation energies difficult. The branches for statistical and direct decay by neutron emission were identified in the spectra. The upper limit for the branching ratio by direct decay (integrated over all observed excitations) was determined to be $20 \pm 6\%$. Even though the statistical uncertainties in the neutron-coincident data were too large to perform detailed studies of the decay by neutron emission from individual states and resonances, the experiment demonstrates the feasibility of the method.

1. Introduction

Studies of spin–isospin excitations in nuclei are important to better understand the isovector spin response of nuclei in general, with applications in astro- and neutrino physics [1–3]. In stellar environments, interactions mediated by the weak nuclear force, such as β-decays, electron captures (ECs), and neutrino-induced reactions, play pivotal roles in the dynamical evolution of supernovae [1] and the crustal heating and cooling of neutron stars [4,5]. ECs are particularly important in these astrophysical environments. They proceed predominantly through Gamow–Teller (GT) transi-

* Corresponding authors.
E-mail addresses: miki@lambda.phys.tohoku.ac.jp (K. Miki), zegers@nscl.msu.edu (R.G.T. Zegers).

http://dx.doi.org/10.1016/j.physletb.2017.04.004

tions and are associated with a change in quantum numbers of $\Delta L = 0$ (angular momentum), $\Delta S = 1$ (spin) and $\Delta T = 1$ (isospin). For pf-shell nuclei, theoretical calculations based on the shell-model or random-phase approximation (RPA) have been studied intensively by comparing with measured B(GT) distributions, primarily extracted from charge-exchange reactions at intermediate energies. Ref. [6] provides an overview of these efforts. In Ref. [7] a new weak-rate library was presented that provides astrophysical modelers with a complete set of electron-capture rates as a function of stellar density and temperature, based on a variety of nuclear structure models. However, for a large fraction of heavy and neutron-rich nuclei, EC rates based on an approximation [8,9] must be used, since rates based on microscopic calculations are not available. This approximation assumes the population of a single state through a Gamow–Teller excitation with fixed strength and excitation energy that are deduced from a comparison with nuclei in the pf-shell [9]. For heavier neutron-rich nuclei, this approximation will overestimate the EC rates, as the increasing effects of Pauli blocking are not considered. Although the approximation was recently improved [10] by adding dependencies to isospin and odd–even effects, the longer-term goal is to improve the library by including rate sets for heavier nuclei that are based on microscopic calculations and benchmarked by experimental data in a similar fashion as was done for nuclei in the pf shell. In this work, the GT transition strengths in the $\beta+$/EC direction from ^{100}Mo were extracted by studying the ^{100}Mo$(t, {}^3$He) charge-exchange reaction at 115 MeV/u with the goal to test microscopic models that are candidates for providing rate sets of EC for heavier nuclei in the weak-rate library. ^{100}Mo is slightly outside of the region of nuclei that is expected to contribute strongly to the deleptonization process of the core in core-collapse supernovae [7,11]. Nevertheless, until a method to study GT strengths in the EC direction on unstable neutron-rich nuclei is developed, ^{100}Mo as the most neutron-rich stable Molybdenum isotope, is a good case for testing modern theoretical models in the medium-heavy neutron-rich mass region.

The operator for the isovector spin giant monopole resonance (IVSGMR) [12–19] carries the same ΔL, ΔS and ΔT as the GT operator, but the IVSGMR is a $2\hbar\omega$ excitation, whereas the GT excitation is of $0\hbar\omega$ nature. Hence, the IVSGMR appears at higher excitation energies. In a macroscopic picture of the nucleus, it is described as the out-of-phase oscillation of neutron and proton densities. Therefore, by measuring the properties of the IVSGMR one gains insights into the bulk, as well as the microscopic properties of the isovector response of nuclei at high excitation energies. A measurement of the IVSGMR excited through the ^{100}Mo$(t, {}^3$He) charge-exchange reaction adds to the slowly increasing body of experimental data from $(t, {}^3$He) experiments for this resonance [13–16,20]. The charge-exchange (CE) $(t, {}^3$He) reaction is a powerful spectroscopic tool for studying the β^+ spin–isospin excitations, including the GT and IVSGMR excitations. In addition to the unambiguous isovector selectivity, at intermediate incident energies it predominantly induces spin-transfer transitions [2,21,22]. The GT transition strength is reliably extracted from the CE cross section through the well-studied and calibrated proportionality between GT strength and differential cross section at small linear momentum transfer ($q \approx 0$) [3,23–25].

Nuclei excited at higher energies than their particle-emission threshold will predominantly decay via the emission of a particle. The observation of CE reactions in coincidence with decays by neutron or proton emission provides deeper insights of the spin–isospin excitations in the continuum [13,20,26–30]. The decay by particle emission is either direct, in which case the particle escapes from the $1p$-$1h$ doorway state to leave behind a hole state, or statistical, in which case the excited state couples to many-particle, many-hole configurations and the nucleus achieves thermal equilibrium prior to the emission of a particle [19]. From the study of the direct-decay process, detailed information about the microscopic structure of the excited state is obtained as the residual hole state reflects the composition of the original particle-hole configuration. The competition between direct and statistical decay processes has been studied quite extensively (in theory and experiment) in the β^- channel [13,20,26,28,31–37], in which proton-particle, neutron-hole excited states are populated in the CE reaction. In that case, the direct decay is associated with the emission of a proton with an energy in excess of the Coulomb barrier and the statistical decay is associated with the emission of low-energy neutrons and photons. Similar studies have not yet been performed in the β^+ channel, in which neutron-particle, proton-hole states are populated. Hence, the statistical and direct decay processes are expected to be primarily associated with the emission of neutrons and only separable through a measurement of the energy of the emitted neutrons. In this study, we measured the neutron decay from ^{100}Nb excited in the ^{100}Mo$(t, {}^3$He$)^{100}$Nb reaction and extracted first results for the branching ratio for decay by direct neutron emission.

2. Experiment

The ^{100}Mo$(t, {}^3\text{He} + n)$ experiment was performed at the Coupled Cyclotron Facility (CCF) at NSCL. The primary ^{16}O beam was accelerated to 150 MeV/u with a radio frequency of 23.833 MHz and struck a ^{9}Be production target. Among the reaction products, tritons of 115 MeV/u were selected with a momentum acceptance ($\Delta p/p$) of 0.5% in the A1900 fragment separator and purified to better than 99% by using a 195 mg/cm^2 Al wedge placed in the intermediate image of the A1900. The triton beam intensity was 10^7 pps on average. It was monitored by correlating the current of the ^{16}O primary beam, which was measured by a non-intercepting probe placed just after the CCF, with the yield measured for the ^{12}C$(t, {}^3$He$)^{12}$B$(1^+$,g.s.) reaction. The cross section for this reaction was determined previously [23] and was, therefore, used to determine the ratio of the triton beam intensity to the ^{16}O primary beam intensity.

The beam struck a ^{100}Mo target with a thickness of 10 mg/cm^2. The ^{3}He particles scattered at forward angles were momentum-analyzed by the S800 spectrometer and detected in its focal plane by cathode-readout drift chambers and a plastic scintillator. The excitation energy in ^{100}Nb was determined in a missing-mass calculation with a resolution of 500 keV (FWHM). Details of the experimental methods are found in Ref. [38].

Neutrons emitted in the decay of the excited ^{100}Nb nuclei were detected by two types of neutron detectors surrounding the ^{100}Mo target. One type consisted of the plastic-scintillation detector arrays (referred to as LV, hereafter) LENDA [39,40] (24 bars with dimensions of 4.5 cm (W) × 2.5 cm (D) × 30 cm (H)) and part of VANDLE [41,42] (24 bars with dimensions of 3 cm (W) × 3 cm (D) × 60 cm (H)). The plastic scintillator bars were installed vertically at a distance of 1 m from the target, with their centers at the same height as the target, and covering scattering angles between 64° and 161° with partially overlapping intervals of 4.2°. The second type consisted of a small liquid-scintillator array (LS, hereafter). It had 8 detectors with a diameter of 5.08 cm and a depth of 5.08 cm. The detectors were placed in a vertical plane around the target, at a distance of 15 cm, and covering scattering angles between $51° \leq \theta \leq 129°$ in intervals of 26°. The time-of-flight (TOF) resolution as determined from the prompt-coincidence events in which a photon was emitted was 900 ps (FWHM). The TOF resolution was limited by the precision of the start timing pro-

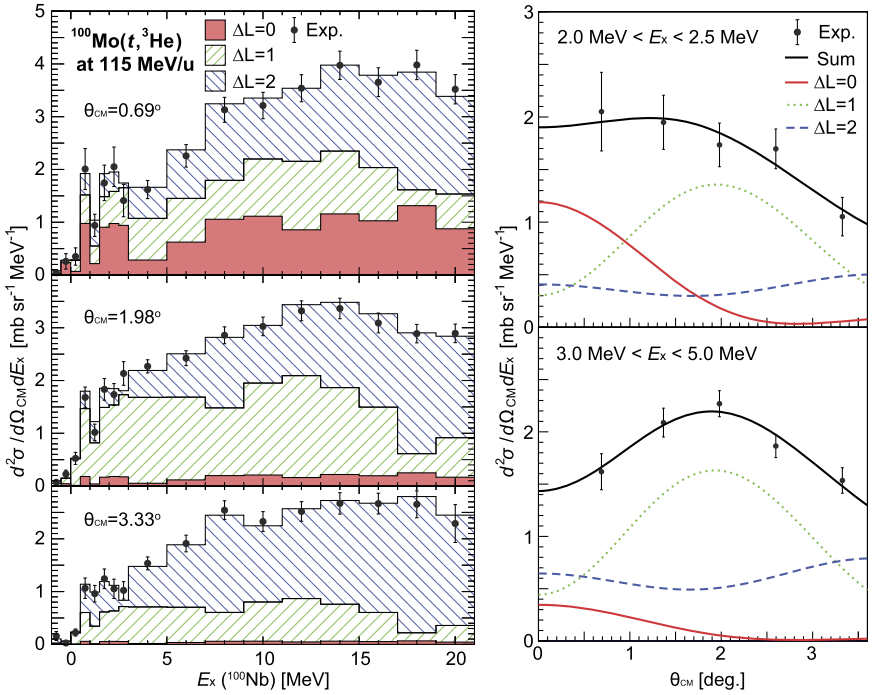

Fig. 1. (Color online.) The measured double differential cross sections and the results of the MDA for the ^{100}Mo(t, ^{3}He) reaction at 115 MeV/u. The left panel shows the cross section as a function of excitation energy for $\theta_{CM} = 0.69$, 1.98 and 3.33°. The right panel shows examples of the MDA for the excitation-energy bins $E_x = 2.0$–2.5 and $E_x = 3.0$–5.0 MeV. The black points are the experimental data. The error bars shown are statistical in nature only. See text for systematic errors.

vided by the S800 focal-plane scintillator, and corrected for the TOF of the ^{3}He particle in the spectrometer.

3. Singles data

The measured double-differential cross sections for the ^{100}Mo(t, ^{3}He) reaction are shown by the black points in Fig. 1. The systematic error is 11%, which comes mainly from the uncertainty in the intensity of the incident triton beam. A multipole decomposition analysis (MDA) was performed for extracting the contributions for excitations associated with different units of angular momentum transfer (ΔL). Only components with $\Delta L \leq 2$ were included in the MDA. For (t,^{3}He) studies at forward scattering angles it has been found that the inclusion of a component with $\Delta L = 3$ generally does not improve the quality of the fit as its angular distribution is easily mimicked by a $\Delta L = 2$ component and a weak $\Delta L = 1$ component. Hence, given the limited statistics, a component with $\Delta L = 3$ was not included in the fit. The cross sections were calculated by the computer program FOLD [43]. The nucleon–nucleon interaction was taken from the t-matrix parameterization at 140 MeV by Love and Franey [22]. The ^{3}He and t densities were obtained from variational Monte Carlo results [44]. The target transition density was calculated based on the normal-modes procedure by using the code NORMOD [45]. The optical potential was taken from the experimental parameter sets for the ^{3}He + ^{90}Zr scattering at 148 MeV/u [46].

The results of the MDA are shown in Fig. 1. The obtained $\Delta L = 0$ component has a small bump around $E_x = 2$ MeV, associated with the $0\hbar\omega$ GT excitations, and a broader structure at the higher excitation energies, dominated by the excitation of the $2\hbar\omega$ IVSGMR. For the comparison with theoretical calculations, the experimental cross sections were converted into transition strengths by using the proportionality relation:

$$d\sigma_i/d\Omega|_{CM;\theta=0^\circ} = \hat{\sigma}_i F_i(q) B \text{ (i)} \quad (i = \text{GT, IVSGMR}), \tag{1}$$

where $\hat{\sigma}_i$ is the unit cross section and $F_i(q)$ is the kinematic correction factor calculated by FOLD. The unit cross section $\hat{\sigma}_{GT}$ was obtained, with a $\sim 10\%$ uncertainty, from the well-established empirical relationship with mass number [3,23], while the $\hat{\sigma}_{IVSGMR}$ was obtained by the FOLD calculation. The latter was corrected by 10% based on the difference between the calculated unit cross section in FOLD and the empirical unit cross section for the GT strength. As the proportionality between IVSGMR strength and cross section has not been well established, the unit cross section for the IVSGMR carries an estimated uncertainty of at least 30%.

The GT and IVSGMR strength distributions are shown in the top and bottom panels of Fig. 2, respectively. Since the GT and IVSGMR excitations are both associated with $\Delta L = 0$, they cannot be separated on the basis of the MDA. Separation can only be done by comparing the same excitations in a reaction with a less absorptive probe, such as the (n,p) reaction, as was done for the cases of ^{90}Zr and ^{208}Pb [15]. Therefore, the results shown in Fig. 2 are based on a simple assumption that the cross sections associated with $\Delta L = 0$ at the low (high) excitation energies are due to the excitation of GT states (IVSGMR).

The logft value [47] for the β decay from ^{100}Nb(g.s.) to ^{100}Mo(g.s.) is 5.1 ± 0.1, corresponding to $B(\text{GT}) = 0.09 \pm 0.02$. Our experimental result gives 0.04 ± 0.03 for $|E_x| < 0.5$ MeV, which is consistent with the β decay result within the uncertainties. The total GT strength up to 4 MeV is $\sum B(\text{GT}) = 0.77 \pm 0.13$ (stat.) $\pm$ 0.08 (syst.).

4. Theoretical framework

For the total Gamow–Teller transition strength, a simple estimate was made by using a single-particle model (s.p.) [48] under the assumption that in ^{100}Mo two protons occupy the $g_{9/2}$ orbit and the neutron $g_{7/2}$ orbit is completely empty. The B(GT) in this case amounts to 3.55. This estimate does not take into account possible quenching mechanisms, which are discussed below. It is

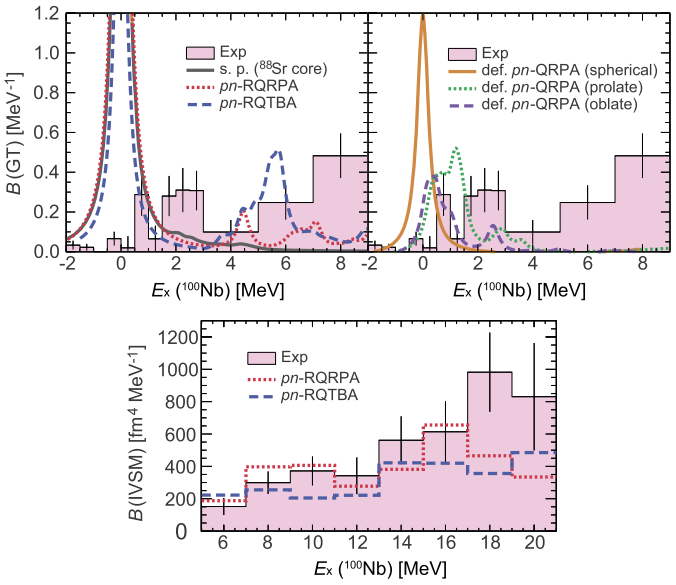

Fig. 2. (Color online.) The GT (top) and IVSGMR (bottom) strength distributions. The histograms (pink with black borders) are the experimental results and the error bars are statistical in nature only. The curves represent the theoretical calculations. See text for details. Two plots are presented for the GT strength distribution, where different types of theoretical calculations are shown together with the same experimental data.

useful to compare the sophisticated approaches described below with this estimate as a reference.

A theoretical description of the GT and IVSGMR excitations in ^{100}Mo was developed by using a proton–neutron version of the relativistic quasiparticle time-blocking approximation (*pn*-RQTBA) [49]. It is based on the effective meson-exchange interaction between nucleons while the meson masses and coupling constants are slightly adjusted to bulk nuclear properties on the Hartree level. The latter forms the content of the covariant energy density functional theory (CEDFT) [50], which serves as a basis for calculations of the nuclear response function. The basis single-quasiparticle states are 8-component Dirac spinors obtained as solutions of the relativistic Hartree–Bogoliubov problem, which in the case of the monopole pairing force reduces to the relativistic Hartree-BCS. The Bethe–Salpeter equation (BSE) for the nuclear response function is formulated in this basis and projected onto the proton–neutron channel. Similar to the RQTBA in the neutral channel [51], the kernel of the BSE, besides the static part, also contains the energy-dependent part, which describes exchanges of vibrational quanta between nucleons, known as quasiparticle-vibration coupling (QVC). These vibrations represent oscillations formed by collective coherent motion of strongly-interacting nucleons, and produce an effective boson-exchange interaction giving the leading-order contribution to the energy-dependent interaction. The frequencies of these vibrations and their coupling vertices are calculated in the self-consistent relativistic quasiparticle random phase approximation (RQRPA) [52] with NL3 [53] interaction based on the same version of the CEDFT, providing a closed self-consistent calculation scheme for *pn*-RQRPA. In the present version of the model for isospin-transfer excitations, ρ-meson and pion exchanges become responsible for the static part of the interaction, as described in [37,54–56]. The calculations are performed with (*pn*-RQTBA) and without (*pn*-RQRPA) QVC, in order to illustrate its impact on the GT and IVSGMR excitations.

Calculations that consider the deformation of ^{100}Mo were also performed by using a deformed *pn*-QRPA framework, in which the transition strength was obtained using the proton–neutron finite-amplitude method (pnFAM) [57] on top of an axially-deformed Hartree–Fock–Bogoliubov mean field computed with the HFBTHO code [58]. The model space consisted of the first 16 harmonic-oscillator major shells and the interaction was SkO' [59], fine-tuned to better reproduce Gamow–Teller and spin-dipole resonances and beta-decay half-lives across the nuclear chart in Ref. [60]. Both a prolate and an oblate minimum were found for the ^{100}Mo mean field. The oblate minimum ($\beta_2 = -0.195$) had the lower total energy of -853.053 MeV and the prolate minimum ($\beta_2 = 0.227$) had a total energy of -852.609 MeV. For comparison, the solution with the mean field constrained to be spherical was also computed, and found to have the energy of -851.798 MeV. The ground state of ^{100}Nb was estimated by computing the transition strength with a narrow smearing at low energies and identifying the lowest-energy peak in the strength function. While this procedure is not generally applicable, as the lowest-energy peak can go unnoticed if there is little transition strength between the ground states or if the transition is forbidden, in this particular case we justify it by the available experimental data on ^{100}Nb beta decay [47], as discussed above. As the QRPA describes the linear response of a mean field, it is limited to a single mean field, which in our computations is a spherical, or at most an axially-deformed one. To further improve the description one should take into account the gamma-softness of ^{100}Mo, using a model that does not rely on the mean-field approximation. Finally, we note that the effective axial vector coupling constant of $g_A = 1.0$ [60] has been adopted consistently in the *pn*-(R)QRPA and *pn*-RQTBA calculations.

5. Comparison

In the top panel of Fig. 2, the s.p. estimate and *pn*-RQRPA calculations for the GT strength distribution are compared to the experimentally extracted GT strength at low excitation energies. The theoretical estimates have been smeared with the experimental resolution. The s.p. estimate ($B(\mathrm{GT}) = 3.55$) and the *pn*-RQRPA calculation with a summed $B(\mathrm{GT}) = 3.88$ are nearly consistent. In the *pn*-RQTBA calculation, the summed GT strength is lower ($B(\mathrm{GT}) = 3.11$), and some of the strength is pushed up in excitation energy. In Ref. [61], the measured $B(\mathrm{GT})$ distribution for the ^{98}Cd β decay was compared with the shell-model calculations. The observed strength was found to be quenched relative to the calculations by a factor of 4. If the same factor is applied to the s.p. estimate, the total GT strength becomes 0.83, which is consistent with the present experimental results when integrated up to 4 MeV. The origin of this quenching was attributed to the multi-particle-multi-hole and delta-particle-nucleon-hole admixtures in Ref. [61]. By comparing the *pn*-RQRPA calculations with the *pn*-RQTBA calculations, one finds that the inclusion of QVC results in a quenching of the low-lying strength and an increase of strength at higher excitation energies, where it becomes almost indistinguishable from the IVSGMR. The *pn*-QRPA calculations, with a tunable $T = 0$ proton–neutron pairing interaction based on Ref. [59,60] produced a stronger quenching of the strength than the s.p. estimate and the *pn*-RQRPA calculations where the isoscalar proton–neutron pairing is not included, even if deformation is not considered. The spherical calculation gives a total strength of 0.82, almost entirely associated with the transition to the ground state of ^{100}Nb. By including deformation effects, the strength distributions become fragmented and comparable to the experimental results, even if the details of the data are not well reproduced. In the case of the prolate (oblate) minimum, the total GT strength is 0.85 (0.53), both consistent with the data. It is concluded that the consideration of deformation effects and isoscalar proton–neutron pairing is crucial in order to make better estimates for the Gamow–Teller transition strengths.

As shown in the bottom panel of Fig. 2, the theoretical IVSGMR strength distributions calculated in the *pn*-RQRPA and *pn*-RQTBA

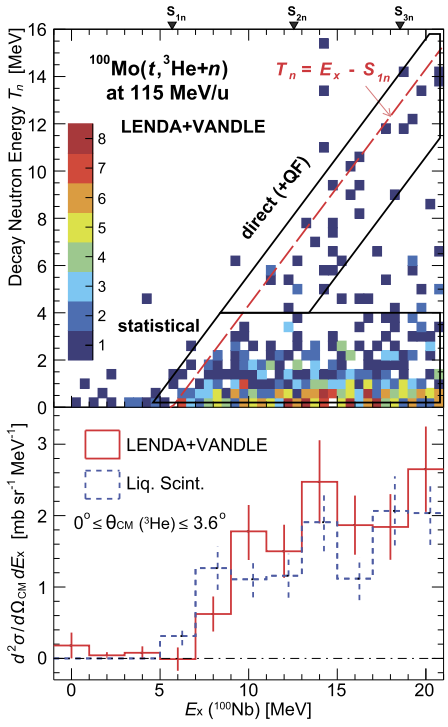

Fig. 3. (Color online.) The ^{100}Mo(t, ^{3}He + n) spectra. The top panel shows the yield distribution as a function of the ^{100}Nb excitation energy and the energy of the emitted neutron measured by the LV system. The gates shown by the black lines are used for calculating the branching ratio for direct and statistical decays, as detailed in the text. The bottom panel shows the neutron-coincident double differential cross sections for the LV and LS systems.

formalisms are roughly consistent with the data over the measured excitation-energy region, except near 20 MeV, where the data overshoots the theoretical estimates. In this panel, the extracted strengths were binned in the same manner as the experimental data.

6. Neutron coincidence data

The ^{100}Mo(t, ^{3}He + n) coincidence spectra are shown in Fig. 3. The top panel shows the yield distribution as a function of the excitation energy (E_x) of ^{100}Nb and the neutron energy (T_n) measured in the LV system. The spectrum consists of a statistical-decay component, and a direct-decay component. Based on a statistical-decay calculation by using the code CASCADE [62], it was found that this component is associated with low-energy neutrons ($T_n <$ 4 MeV), independent of the excitation energy of ^{100}Nb. The direct decay component follows a diagonal pattern as $E_x - T_n - S_{1n}$ represents the excitation energy of the residual nucleus, where S_{1n} is the neutron separation energy. The dashed red line corresponds to the decay from excited ^{100}Nb states to the ground state of ^{99}Nb. The few events that appear significantly above this line stem from accidental coincidences (occurring at $\sim$ 5% of the prompt coincident rate) and possibly some scattering of neutrons in surrounding materials. They were rejected in the following analysis. We note that neutrons produced in the quasi-free (QF) processes [13, 28] also contribute to the same kinematical region as the direct decay component. The neutrons from the QF processes are emitted predominantly at very forward scattering angles and can be distinguished from neutrons emitted in the decay processes by investigating the angular distribution [13,28]. However, given the limited statistics, it was not possible to meaningfully perform such an analysis in the present work.

The bottom panel in Fig. 3 shows the neutron-coincident double-differential cross section measured with the LV (solid) and LS (dashed) systems. To obtain these cross sections, a correction was applied to account for the intrinsic and geometrical efficiencies of the neutron detectors. The intrinsic neutron efficiencies of LV scintillator bars were simulated by the GEANT4 toolkit with the high-precision (HP) neutron cross-section package, covering neutron energies up to 20 MeV. For the LS system, the program NEFF7 [63] was used to calculate the intrinsic efficiencies. The geometrical efficiency was determined by assuming an isotropic angular distribution of the emitted neutrons. As mentioned above, it was not possible to verify this assumption with good precision. The total efficiency was about 2.3% (0.9%) at $T_n = 1$ MeV ($T_n = 10$ MeV) for the LV system, for which the thresholds were set (in software) to 40 keVee. The efficiencies for LS system were 2.6% (0.7%) at $T_n = 1$ MeV ($T_n = 10$ MeV) with thresholds set (in software) to 32 keVee.

The neutron-coincident cross sections are typically 60% of the singles cross section shown in Fig. 1. This is at least partially due to the fact that some neutrons have energies that are below the thresholds of $T_n \approx 400$ keV set in the analysis. Based on the above-mentioned statistical-decay calculation with the code CASCADE [62], 10–20% of events will have been missed because of these thresholds. Anisotropicities in the neutron angular distributions also affect the extracted coincident cross section data. Finally, it is also possible that for a fraction of the events the decay proceeds entirely by γ or proton emission and neutrons are not emitted.

The branching ratio for the direct-decay component, determined from the efficiency-corrected yield in the "direct" gate in Fig. 3, was $20 \pm 6\%$. As mentioned above, it includes contributions from QF process, which makes this percentage an upper limit for the direct decay branch. The direct decay with $T_n < 4$ MeV was not clearly separated from the statistical decay due to the limited yield, and was not included in the "direct" gate. A more detailed analysis requires higher statistics, as was for example done in Ref. [64].

There are some events observed below the direct-decay gate in Fig. 3, but above the statistical-decay gate. These events are likely associated with a semi-direct decay process, in which the excited nucleus emits the neutron prior to reaching full statistical equilibrium [19], or with the population of deep hole states in the direct-decay process [13].

Calculations for the direct decay by neutron emission from the different states/resonances in ^{100}Mo are not available. Predictions in the framework of the Continuum Random Phase Approximation (CRPA) for the direct decay by neutron emission of the IVSGMR populated in $\Delta T_z = +1$ direction from ^{48}Ca and ^{208}Pb give branching percentages of 75% and 46%, respectively [32,33]. It is worth noting that theoretical calculations in the same framework were able to produce experimental results for the direct decay by proton emission from isovector giant resonances populated in the $\Delta T_z = -1$ direction on ^{208}Pb reasonably well [13,20,28,31–34], with branching percentages ranging from $\sim$ 5% for the Gamow–Teller Resonance to $\sim$ 50% for the IVSGMR. Although the present experiment shows the feasibility of performing (t, ^{3}He + n) experiments with the goal of studying the decay properties of the giant resonances populated in the $\Delta T_z = +1$ reaction, better statistics are clearly required to estimate detailed branching ratios for different resonances and to perform meaningful tests of theoretical models.

7. Conclusion

The excitation and decay of the spin–isospin excitations in ^{100}Nb were studied via the ^{100}Mo(t, ^{3}He + n) reaction. It was found that the Gamow–Teller transition strengths are strongly frag-

mented and reduced compared to the single-particle estimate and spherical *pn*-(R)QRPA and *pn*-RQTBA calculations. By including deformation and adjustable proton–neutron pairing interaction in the *pn*-QRPA calculations, a better description of the Gamow–Teller strength at low excitation energies was achieved. Clearly, if one aims to estimate reliable weak-reaction rates based on theoretical calculations for medium-heavy nuclei for inputs to astrophysical simulations, one has to consider the effects of deformation and isoscalar proton–neutron pairing.

At excitation energies beyond ~ 4 MeV, the IVSGMR contributes dominantly to the observed monopole strength. Although its strength distribution is relatively well described by the *pn*-RQRPA and *pn*-RQTBA calculations, the relatively strong excitation of this $2\hbar\omega$ resonance makes it very difficult to extract weak Gamow–Teller transition strengths at higher excitation energies. Such effects constitute a significant challenge for future studies that aim to extract Gamow–Teller strengths from even more neutron-rich (unstable) medium-heavy and heavy nuclei.

The feasibility of performing studies of the decay by neutron emission from giant resonances populated via $\Delta T_z = +1$ charge-exchange reactions was shown, even though the statistical uncertainties in the present experiment were too large to draw conclusions on the branching ratios for decay by direct and statistical neutron emission from individual resonances. Nevertheless, as the study of decay by direct particle emission provides an avenue to better understand the microscopic properties of the giant resonances, the present results stimulate further work in this direction.

Acknowledgements

The authors appreciate the efforts by staff and operators of the CCF facility, A1900 fragment separator and the data acquisition system at NSCL. Enlightening discussions with P. Ring, V. Tselyaev, and V. Zelevinsky are gratefully acknowledged. The authors are very thankful to T. Marketin for providing a part of the code for *pn*-RQRPA matrix elements. This work was supported by the US National Science Foundation [PHY-1102511, PHY-1430152 (JINA Center for the Evolution of the Elements), PHY-1068217, and PHY-1404343], by the US DOE [DE-FG-0291-ER-40608], and by the Japanese Society for the Promotion of Science Postdoctoral Fellowship program for Research Abroad.

References

[1] K. Langanke, G. Martínez-Pinedo, Rev. Mod. Phys. 75 (2003) 819.
[2] M. Ichimura, H. Sakai, T. Wakasa, Prog. Part. Nucl. Phys. 56 (2006) 446.
[3] R.G.T. Zegers, et al., Phys. Rev. Lett. 99 (2007) 202501.
[4] S. Gupta, et al., Astrophys. J. 662 (2007) 1188.
[5] H. Schatz, et al., Nature 505 (2014) 62.
[6] A.L. Cole, et al., Phys. Rev. C 86 (2012) 015809.
[7] C. Sullivan, et al., Astrophys. J. 816 (2016) 44.
[8] G.M. Fuller, W.A. Fowler, M.J. Newman, Astrophys. J. 293 (1985) 1.
[9] K. Langanke, et al., Phys. Rev. Lett. 90 (2003) 241102.
[10] A.R. Raduta, F. Gulminelli, M. Oertel, Phys. Rev. C 95 (2017) 025805.
[11] W. Hix, et al., Phys. Rev. Lett. 91 (2003) 201102.
[12] D. Prout, et al., Phys. Rev. C 63 (2000) 014603.
[13] R.G.T. Zegers, et al., Phys. Rev. Lett. 90 (2003) 202501.
[14] J. Guillot, et al., Phys. Rev. C 73 (2006) 014616.
[15] K. Miki, et al., Phys. Rev. Lett. 108 (2012) 262503.
[16] C.J. Guess, et al., Phys. Rev. C 83 (2011) 064318.
[17] N. Auerbach, A. Klein, Phys. Rev. C 30 (1984) 1032.
[18] I. Hamamoto, H. Sagawa, Phys. Rev. C 62 (2000) 024319.
[19] M.N. Harakeh, A. van der Woude, Giant Resonances, Oxford University Press, 2001.
[20] R.G.T. Zegers, et al., Phys. Rev. C 63 (2001) 034613.
[21] W.G. Love, M.A. Franey, Phys. Rev. C 24 (1981) 1073.
[22] M.A. Franey, W.G. Love, Phys. Rev. C 31 (1985) 488.
[23] G. Perdikakis, et al., Phys. Rev. C 83 (2011) 054614.
[24] M. Sasano, et al., Phys. Rev. C 79 (2009) 024602.
[25] T.N. Taddeucci, et al., Phys. Rev. C 25 (1982) 1094.
[26] R.G.T. Zegers, et al., Phys. Rev. C 61 (2000) 054602.
[27] M. Harakeh, et al., Nucl. Phys. A 577 (1994) 57.
[28] H. Akimune, et al., Phys. Rev. C 52 (1995) 604.
[29] T. Inomata, et al., Phys. Rev. C 57 (1998) 3153.
[30] K. Hara, et al., Phys. Rev. C 68 (2003) 064612.
[31] H. Akimune, et al., Phys. Rev. C 61 (1999) 011304.
[32] I.V. Safonov, N.G. Urin, Bull. Russ. Acad. Sci., Phys. 73 (2009) 858.
[33] M.H. Urin, Phys. At. Nucl. 74 (2011) 1189.
[34] I.V. Safonov, M.H. Urin, Phys. At. Nucl. 75 (2012) 1481.
[35] G. Colò, et al., Phys. Lett. B 276 (1992) 279.
[36] G. Colò, et al., Phys. Rev. C 50 (1994) 1496.
[37] G. Colò, N. Van Giai, Phys. Rev. C 53 (1996) 2201.
[38] G.W. Hitt, et al., Nucl. Instrum. Methods A 566 (2006) 264.
[39] G. Perdikakis, et al., Nucl. Instrum. Methods A 686 (2012) 117.
[40] S. Lipschutz, et al., Nucl. Instrum. Methods A 815 (2016) 1.
[41] W.A. Peters, et al., Nucl. Instrum. Methods A 836 (2016) 122.
[42] S. Paulauskas, et al., Nucl. Instrum. Methods A 737 (2014) 22.
[43] J. Cook, J.A. Carr, Computer program FOLD, Florida State University, unpublished, based on F. Petrovich, D. Stanley, Nucl. Phys. A 275 (1977) 487, modified as described in J. Cook, et al. Phys. Rev. C 30 (1984) 1538, R.G.T. Zegers, S. Fracasso, G. Colò, 2006, unpublished.
[44] S.C. Pieper, R.B. Wiringa, Annu. Rev. Nucl. Part. Sci. 51 (2001) 53.
[45] S.Y. van der Werf, Computer code NORMOD, unpublished.
[46] J. Kamiya, et al., Phys. Rev. C 67 (2003) 064612.
[47] B. Singh, Nucl. Data Sheets 109 (2008) 297.
[48] M.H. MacFarlane, Phys. Lett. B 182 (1986) 265.
[49] C. Robin, E. Litvinova, Eur. Phys. J. A 52 (2016) 205.
[50] D. Vretenar, et al., Phys. Rep. 409 (2005) 101.
[51] E. Litvinova, P. Ring, V.I. Tselyaev, Phys. Rev. C 78 (2008) 014312.
[52] N. Paar, et al., Phys. Rev. C 67 (2003) 034312.
[53] G.A. Lalazissis, J. Koñig, P. Ring, Phys. Rev. C 55 (1997) 540.
[54] N. Paar, et al., Phys. Rev. C 69 (2004) 054303.
[55] T. Marketin, et al., Phys. Lett. B 706 (2012) 477.
[56] E. Litvinova, et al., Phys. Lett. B 730 (2014) 307.
[57] M.T. Mustonen, et al., Phys. Rev. C 90 (2014) 024308.
[58] M.V. Stoitsov, et al., Comput. Phys. Commun. 184 (2013) 1592.
[59] P.G. Reinhard, et al., Phys. Rev. C 60 (1999) 014316.
[60] M.T. Mustonen, J. Engel, Phys. Rev. C 93 (2016) 014304.
[61] B.A. Brown, K. Rykaczewski, Phys. Rev. C 50 (1994) R2270.
[62] F. Pühlhofer, Nucl. Phys. A 280 (1977) 267;
Computer code CASCADE, unpublished.
[63] G. Dietze, H. Klein, Computer codes NRESP4 and NEFF4, Physikalisch-Technische Bundesanstalt ND22, 1982. Updated versions NRESP7 and NEFF7, 1991, unpublished.
[64] S. Brandenburg, et al., Phys. Rev. C 39 (1989) 2448.